Prediction of air/oil exit flows in a commercial aero-engine bearing chamber

M Farrall, S Hibberd, K Simmons*, and D Giddings
The University of Nottingham Technology Centre in Gas Turbine Transmission Systems, University of Nottingham, Nottingham, UK

The manuscript was received on 22 June 2005 and was accepted after revision for publication on 4 January 2006.

DOI: 10.1243/09544100JAERO40

Abstract: An understanding and optimization of three-dimensional air/oil flows in aero-engine transmission systems forms an integral part of future designs. This especially applies to bearing chambers, which contain a complex two-phase flow formed by the interaction of sealing air-flows and lubrication oil. A critical design quantity is the composition of the liquid (oil) and gas (air) phases in the exit flows. Using a previously validated numerical model, the air/oil flow in a commercial bearing chamber is computed with particular focus on the flow exiting the chamber. The division of oil exiting the chamber through the vent and scavenge ports is determined for three shaft speeds and two configurations of the vent port. Comparison with available experimental data shows that consistent trends are predicted, but further model development is necessary in the vicinity of the scavenge port.

Keywords: film modelling, two-phase, computational fluid dynamics (CFD), bearing chamber, oil droplet impact, vent port, scavenge port

1 INTRODUCTION

The commercial aero-engine bearing chamber studied comprises a roller bearing, diametrically opposed vent and scavenge exit ports and associated rotating and stationary components. A cross section of the predominantly annular chamber taken at the angular location of the vent pipe is shown in Fig. 1. The high rotation rate of the shaft induces a strong azimuthal airflow. This airflow is modified by flow inlets, through an axisymmetric bearing and seal, and flow outlets, through vent and scavenge pipes. Oil is supplied to the roller bearing for lubrication and as a result, discrete oil droplets are ejected into the rotating airflow. Because angular momentum is transferred to the droplets from the bearing and associated cage, the droplets ultimately impinge on the outer chamber housing. The impingement may result in immediate deposition, in which case a wall film is formed that migrates around the chamber under the influence of the momentum resulting from the impact of oil droplets with the film, together with interfacial shear from the airflow and gravity. Alternatively, droplets may break-up on impact with smaller droplets being ejected back into the airflow and further impingement may occur. The two-phase air/oil mixture then exits the chamber through scavenge and vent ports.

Previous studies into bearing chamber flows have tended to concentrate on one aspect in isolation, such as the oil film motion [**1**–**5**] or the heat transfer [**1**–**7**]. As part of the EU funded project Advanced Transmission and Oil System concepts (ATOS) a computational methodology allowing the analysis of the general two-phase air/oil flows in aero-engine bearing chambers was developed and validated [**8**]. This model is applied to a commercial bearing chamber in the present study and the resulting split of oil exiting the chamber through the vent and scavenge investigated.

2 BEARING CHAMBER MODEL

Simulations of the two-phase flow are based on a commercial computational fluid dynamics (CFD)

Corresponding author: School of Mechanical, Materials, and Manufacturing Engineering, University of Nottingham, University Park, Nottingham, NG7 2RD, UK. email: kathy.simmons@nottingham.ac.uk

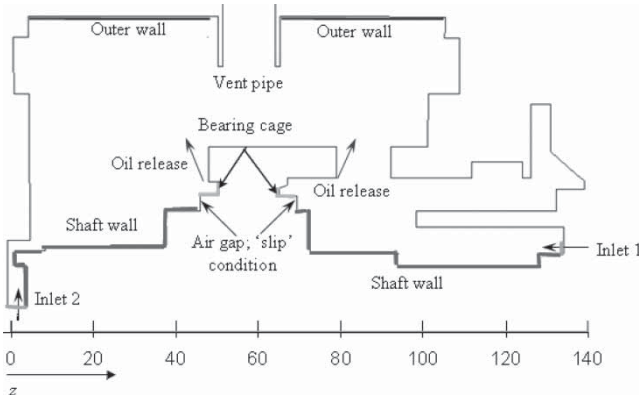

Fig. 1 Schematic of bearing chamber geometry used in CFD model (length scale in mm)

package with in-house sub-models for the calculation of the oil film motion and the interaction of the oil droplets with the oil film. The constituent modules and associated coupling between them are shown in Fig. 2. The computations involve the implementation of successive stages. Firstly, the airflow in the chamber is calculated using the commercial CFD package CFX-4.3. Oil droplets are then tracked through the chamber using a Lagrangian tracking routine, assuming aero-dynamic drag is the dominant force. An in-house module is used to determine the outcome of droplet/film impacts (stick, rebound, spread, splash) on the basis of an impact parameter K ($= We_d^{0.5}\mathrm{Re}_d^{0.25}$) and Weber number. If required, droplets are sourced from the point of impact and the tracking is continued. It is assumed in this calculation that the film thickness is negligible compared with the size of the chamber, so that the surface of the film is taken as corresponding to the chamber wall. Finally, droplet data are gathered for the input of mass and momentum to the oil film. These data are used together with a computed distribution of surface shear, obtained from the CFD solution, to provide required boundary information to the oil film model. The two-dimensional integral model developed by Farrall *et al.* [**4**, **9**] has been employed to account for the dynamics of this wall film. The model assumes an incompressible, isothermal flow and accounts for the effects of gravity, shear forces on both the wall and the film's surface, and the addition of mass and momentum to the film from impinging oil droplets.

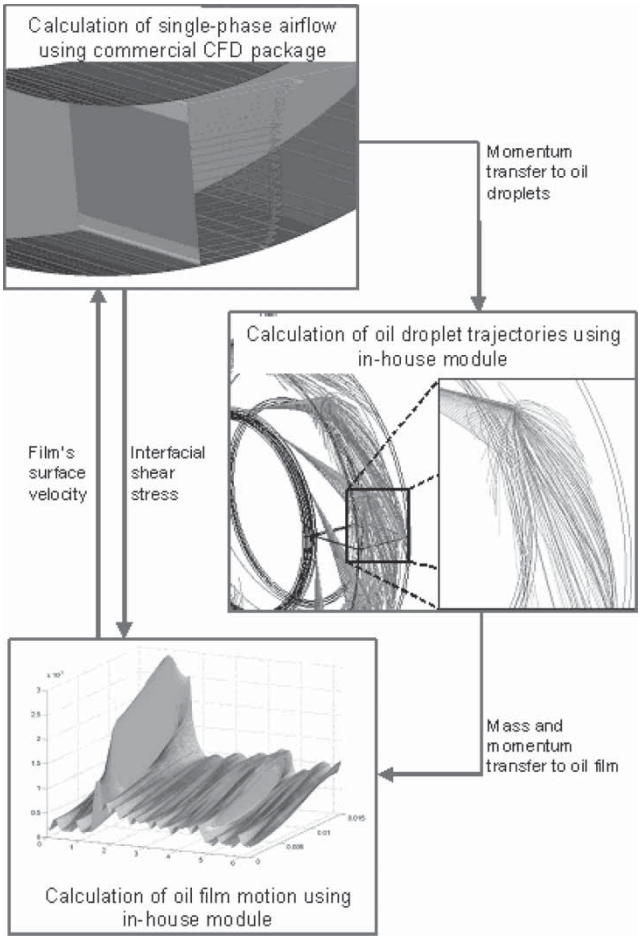

Fig. 2 Flow chart illustrating the different calculations and associated interactions

2.1 Airflow in the chamber

The outline of the computational domain for the CFD model and location of the inlets to the chamber are shown in Fig. 1. It is assumed that negligible air exits the chamber through the scavenge and thus this geometrical feature is omitted in the CFD calculation. The single-phase airflow in the chamber is calculated on a body-fitted structured grid comprising 503 960 cells. An appropriate mesh density was established from previous work on a similar configuration [**8**]. The velocity field is modelled as incompressible and isothermal, and is solved in a Cartesian coordinate system using the standard k–ε turbulence model to calculate the turbulence quantities. The equations were discretized using a higher-upwind differencing scheme and solved using the SIMPLE pressure-correction algorithm. At typical operating conditions of 250 kPa and 343 K [**9**] the air has a density of 2.923 kg/m^3 and a dynamic viscosity of 1.84 Ns/m^2. The shaft rotates with a speed in the range 10 000 to 19 000 r/min and sealing air enters through inlet 1 (see Fig. 1) at a rate of 15 g/s. In the current analysis, it is assumed that the airflow through inlet 2 is negligible.

2.2 Oil droplet motion

On the basis of the typical operating conditions given in reference [**10**], oil is modelled as being shed from

the bearing at a rate of 93 g/s. This oil is injected in the form of droplets, released from 10 equally spaced angular locations on either side of the bearing. On the basis of the experimental data in reference [**11**], the initial distribution of droplet diameters is given by a Rossin–Rammler distribution with a mean of 480 μm and a spread of 3. The initial azimuthal and radial components of each droplet's velocity are taken as equal to that of the local air velocity. In addition, to ensure the droplets leave the wall, an axial component equal to 0.5 m/s, directed away from the bearing, is assumed.

Interactions of the droplets with the oil film on the outer chamber housing are accounted for by an in-house module [**8**, **12**]. On the basis of the local droplet/film conditions, the impacts are primarily divided as to whether splashing occurs, in which case secondary diameters and velocities are determined. If the droplet does not break-up, the impact is further classified into the regimes of stick, rebound, and spread. In the present calculations, droplets are assumed to rebound when they impact with other walls in the chamber.

2.3 Oil film motion

On the basis of the assumption that the film thickness is small compared to the radius of the chamber, simplified equations are solved for mass and momentum, accounting for the effects of interfacial shear, gravity, and source terms associated with the oil droplet impacts [**8**]. Numerical calculations are performed by discretization of the governing equations using the CFLF4 scheme of Liska and Wendroff [**13**]. The effect of geometric features such as the vent and scavenge ports on the film's motion are included through boundary conditions on the basis of a local analysis that incorporates a measure of the restriction to the exiting flow. The computational grid comprises 50 nodes axially and 350 nodes circumferentially, with consideration being given to two limiting cases of vent port configuration, proud and flush to the chamber housing, shown schematically in Fig. 3. A *proud* vent pipe protrudes through the film into the chamber such that the oil film must go around the pipe and cannot exit into the vent. In contrast a vent that is *flush* with the chamber wall allows oil film to exit freely into the pipe.

3 CHARACTERISTICS OF THE OIL DROPLET AND OIL FILM MOTION

Figure 4 shows typical oil droplet trajectories calculated for a shaft speed of 15 000 r/min. Initially, the droplets are dominated by the azimuthal component of the release velocity, proceeding in a straight line to the chamber housing. Interaction with the primary airflow results in some spread of the trajectories for smaller droplet diameters. Initial impacts with the oil film on the chamber housing result in splashing, ejecting secondary droplets back into the core flow. These droplets tend to remain in a region near the outer wall, extending to a depth of about 15 mm (see Fig. 4(b)). It is observed from Fig. 4(a) that there is a concentration of smaller droplets in the region above the bearing with some leaving through the vent port. These smaller droplets, generated through the interaction with the outer chamber wall, have small Stokes number and are thus dominated by the airflow, travelling around the chamber several revolutions before exiting through the vent port. The amount of oil suspended in the air and thus exiting through the vent has been determined as part of the simulation. For the case shown here it was found that 72 per cent of the released oil is transferred to the film by the impinging droplets. It

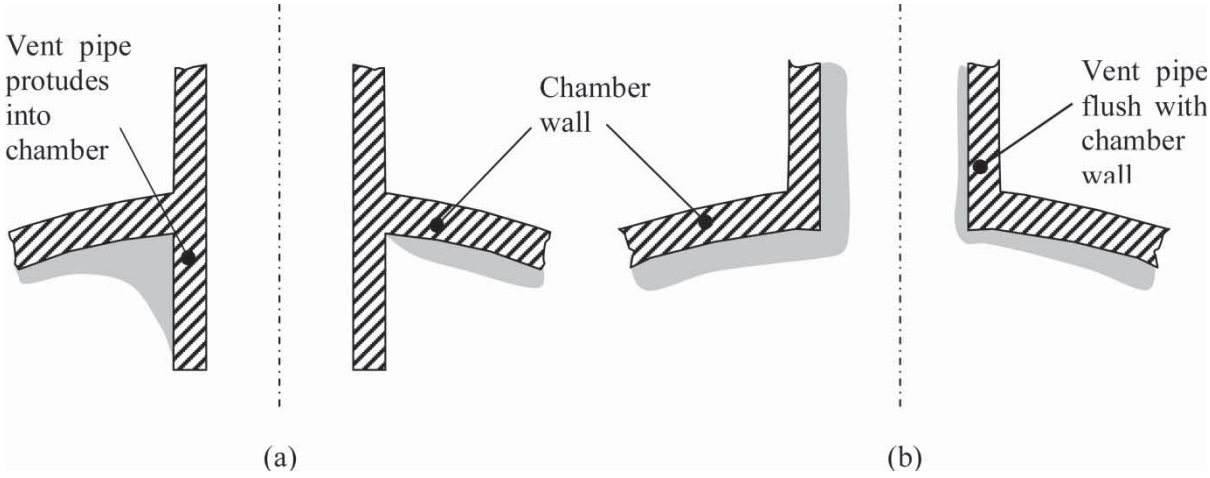

Fig. 3 Vent port configurations investigated: (a) proud and (b) flush

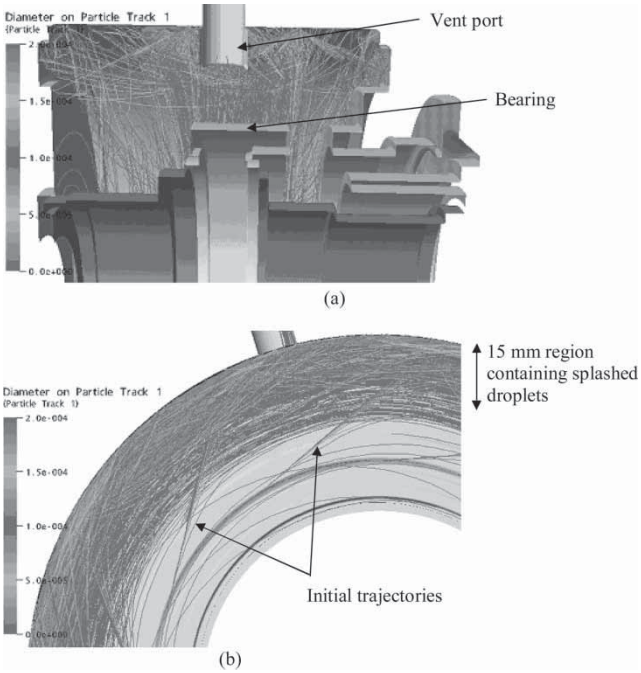

Fig. 4 Oil droplet trajectories shown in (a) a plane through the vent port and (b) an axial plane corresponding to $z = 60$ mm

is thus concluded that 28 per cent is suspended in the core airflow and exits through the vent.

Figure 5 shows the corresponding surface plot of the oil film thickness around the chamber wall, for a flush vent port. The combination of the interfacial shear and momentum supplied by the droplets drives the film around the chamber wall. In addition, there is the gravitational force, which acts to retard the flow on the rising side of the chamber ($3\pi/2 \leqslant \theta \leqslant 2\pi$ and $0 \leqslant \theta \leqslant \pi/2$) and accelerate it on the down side of the chamber. In the absence of any gravitational effect, a uniform film thickness would be observed around the chamber wall.

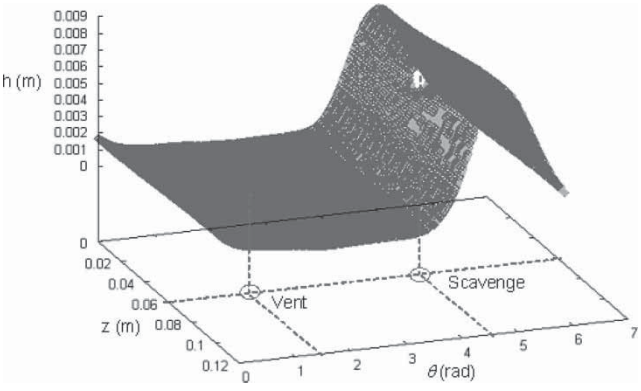

Fig. 5 Film thickness distribution on the outer chamber wall

However, in the present calculations the oil is found to form a pool in the lower half of the chamber indicating that gravity does have an important role. This pooling of the oil could have important implications in terms of residence time of the oil and thus the heat transfer in the chamber. Moreover, the thicker film could promote re-entrainment of oil by the interfacial shear on the film's surface. It is further noted from Fig. 5 that variations in the axial direction are found to be insignificant.

The mass flow rate of oil exiting the chamber through the vent and scavenge ports is also determined as part of the solution. Considering only the oil exiting via the film, it was found that 11 per cent went through the vent and 89 per cent through the scavenge. Including the oil suspended in the core flow, which exits the chamber through the vent, the proportions exiting through the vent and scavenge become 37 and 63 per cent, respectively.

4 EXIT FLOW PREDICTIONS

Calculations have been performed to understand the effect that, changes in the shaft speed and configuration of the vent port have on the split of oil exiting the chamber through the vent and scavenge ports.

4.1 Shaft speed

With the vent port taken as flush with the outer chamber wall, simulations have been performed for shaft speeds of 10 000, 15 000, and 19 000 r/min. Table 1 shows the calculated proportion of the injected oil that remains in the core flow, as well as that exiting the oil film through the vent and scavenge ports. As the shaft speed is increased, a larger momentum is imparted to the oil droplets resulting in higher energy impacts with the film. This generates an increasingly larger number of smaller droplets that are suspended in the core flow as shown in Table 1.

An increase in the oil exiting the film through the vent port is also observed with an increase in the shaft speed. The higher air speed results in a higher interfacial shear stress on the surface of the film. Combined with the increased momentum from the

Table 1 Oil deposition on the film from the splashing routine for three selected shaft speeds

Shaft speed (r/min)	Suspended in core flow (%)	Oil film	
		Vent (%)	Scavenge (%)
10 000	25.2	7.3	67.5
15 000	29.0	8.0	63.0
19 000	33.1	12.8	54.1

impinging oil droplets the driving force in the film is increased; this drives more oil up the rising side of the chamber and decreases the pooling that occurs. Correspondingly, a higher shaft speed produces an increase in the amount of oil exiting the film through the vent.

4.2 Vent port configuration

To establish the effect of changing the vent pipe configuration on the split of oil exiting the chamber, calculations have been repeated for a proud vent pipe. The main consequence of this configuration is that the oil in the film can now only exit the chamber through the scavenge. Results for the proportional split of oil are given in Table 2 for the case of both a proud and flush vent. It is observed that changing the vent from one that is flush with the chamber housing to one that is proud results in a 7 to 13 per cent decrease in the amount of oil exiting the chamber through the vent.

5 DISCUSSION

Some experimental data for the split of oil exiting through the vent and scavenge ports in a commercial bearing chamber containing a ball bearing were obtained during the ATOS programme [**10**]. Although the results of the simulations showed a similar trend to the experimental data, it was found that the quantitative values were considerably higher. In the case of a flush vent, the numerical values predicted an average 33 per cent more oil exiting the chamber through the vent than the experimental data. For the case of a proud vent the over-prediction decreases to around 28 per cent. These differences might result because of the following.

1. Due to late changes in the experimental test program the bearing support differed slightly to that modelled.
2. The initial distributions of droplet diameters and initial velocities have not been accurately determined experimentally and are currently based on the limited experimental data available.
3. The initial conditions for the oil film were taken from previous experimental work on a different rig. The current results suggest that a smaller initial film thickness should be used in the present chamber configuration.
4. The boundary condition used to model the scavenge is simplistic although it appears to work reasonably well in the case of gravity driven flow [**8**]. When the scavenge is pumped, as in a commercial chamber, there are additional fluid effects in the vicinity of the scavenge that are not fully accounted for in the current model.
5. The airflow drawn down the scavenge is not taken as a significant element when determining the oil exiting the chamber. If it is significantly higher than assumed, then modelling this geometric feature in airflow and oil droplet calculation is necessary. One consequence of including the scavenge pipe in the CFD model would be to decrease the predicted proportion of oil exiting the vent in the form of droplets. Currently, airborne droplets are predicted to contribute two-thirds of the oil exiting through the vent.

6 CONCLUSIONS

Simulations of the two-phase air/oil flow in a commercial bearing chamber have been carried out for shaft speeds in the range 10 000 to 19 000 r/min for a fixed oil mass flow rate of 93 g/s. Taking the vent port as being flush with the chamber housing, the division of oil exiting the chamber from the vent and scavenge was determined. Computation indicated that around 40 per cent of oil flux left through the vent and the remaining 60 per cent exited through the scavenge. Increases in the shaft speed resulted in an increased amount of oil leaving through the vent. This was attributed to the increased number of splashed droplets that are generated and remain in the core flow, as well as the increase in the driving force on the film. Changing the vent port configuration such that it is proud to the housing resulted in a decrease of 7 to 13 per cent in the amount of oil exiting through the vent.

Table 2 Percentage split of oil exiting the chamber through the vent and scavenge ports for three selected shaft speeds

	Proud vent		Flush vent	
Shaft speed (r/min)	Percentage to vent	Percentage to scavenge	Percentage to vent	Percentage to scavenge
10 000	25.2	74.8	32.5	67.5
15 000	29.0	71.0	37.0	63.0
19 000	33.1	66.9	45.9	54.1

A comparison with available experimental data for the split of oil exiting the chamber through the vent and scavenge showed that although the correct trends were predicted, quantitative measurements showed discrepancies. A number of possible reasons for this have been highlighted with additional work being required to understand the importance of each.

This case study has established the value of this approach to modelling some of the complex multiphase oil/air behaviour found in aero-engine bearing chambers. However, further work would be required to develop the approach to a generic bearing chamber modelling tool.

ACKNOWLEDGEMENT

The work was supported by the European commission within the research project ATOS, contract G4RD-CT-2000-00391. This financial support is gratefully acknowledged.

REFERENCES

1 **Wittig, S., Glahn, A.,** and **Himmelsbach, J.** Influence of high rotational speeds on heat transfer and oil film thickness in aero engine bearing chambers. *ASME J. Eng. Gas Turb. and Power*, 1994, **116**, 395–401.

2 **Glahn, A.** and **Wittig, S.** Two-phase air/oil flow in aero engine bearing chambers: characterisation of oil film flows. *ASME J. Eng. Gas Turb. and Power*, 1996, **118**(3), 578–583.

3 **Chew, J. W.** Analysis of the oil film on the inside surface of an aero engine bearing chamber housing. International Gas Turbine and Aeroengine Congress and Exhibition, Birmingham, UK, 10–13 June 1996, ASME 96-GT-300.

4 **Farrall, M., Hibberd, S.,** and **Simmons, K.** Computational modelling of two-phase air/oil flow within an aero-engine bearing chamber. Proceedings of the ASME FEDSM 2000, Boston, Massachusetts, USA, 11–15 June 2000.

5 **Gorse, P., Busam, S.,** and **Dullenkopf, K.** Influence of operating condition and geometry on the oil film thickness in aero-engine bearing chambers. Proceedings of the ASME Turbo Expo 2004, Vienna, Austria, 14–17 June 2004.

6 **Glahn, A., Busam, S.,** and **Wittig, S.** Local and mean heat transfer coefficients along the internal housing walls of aero engine bearing chambers. International Gas Turbine and Aero-Engine Congress and Exposition, Colorado, USA, June 1997, ASME 97-GT-261.

7 **Busam, S., Glahn, A.,** and **Wittig, S.** Internal bearing chamber wall heat transfer as a function of operating conditions and chamber geometry. *ASME J. Eng. Gas Turb. Power*, 2000, **122**, 314–320.

8 **Farrall, M., Simmons, K., Hibberd, S.,** and **Gorse, P.** A numerical model for oil film flow in an aero-engine bearing chamber and comparison with experimental data. ASME Turbo Expo 2004, Power for Land, Sea and Air, Vienna, Austria, 14–17 June 2004, GT 2004-53698.

9 **Farrall, M., Hibberd, S.,** and **Simmons, K.** Modelling oil droplet/film interaction in an aero-engine bearing chamber. ICLASS-2003, Sorento, Italy, 2003.

10 **Flouros, M.** Test results of scavenge/vent port and mesh variations. *Advanced transmission and oil systems concepts*, Brite Euram Contract G4RD-CT-2000-00391, ATOS report R-WP2-D26-ISS01, 2004.

11 **Wittig, S.** and **Busam, S.** LUBSEAL final test result report, Private communication, University of Karlesrühe, Germany, 1997.

12 **Farrall, M.** *A numerical model for the two-phase flow in a simplified bearing chamber*. PhD Thesis, University of Nottingham, UK, 2000.

13 **Liska, R.** and **Wendroff, B.** Two-dimensional shallow water equations by composite schemes. *Int. J. Numer. Meth. Fluids*, 1999, **30**, 461–479.